# Permeability characteristics of cultured endothelial cell monolayers

STEVEN M. ALBELDA, PHYLLIS M. SAMPSON, FREDERICK R. HASELTON, JUDITH M. McNIFF, STEPHEN N. MUELLER, STUART K. WILLIAMS, ALFRED P. FISHMAN, AND ELLIOT M. LEVINE

*Cardiovascular-Pulmonary Division, Department of Medicine, University of Pennsylvania, and The Wistar Institute and Department of Surgery, Thomas Jefferson University, Philadelphia, Pennsylvania 19104-4283*

ALBELDA, STEVEN M., PHYLLIS M. SAMPSON, FREDERICK R. HASELTON, JUDITH M. McNIFF, STEPHEN N. MUELLER, STUART K. WILLIAMS, ALFRED P. FISHMAN, AND ELLIOTT M. LEVINE. *Permeability characteristics of cultured endothelial cell monolayers.* J. Appl. Physiol. 64(1): 308–322, 1988.—The purpose of this study was to characterize the permeability characteristics of an in vitro endothelial cell monolayer system and relate this information to available in vivo data. We cultured bovine fetal aortic endothelial cells on fibronectin-coated polycarbonate filters and confirmed that our system was similar to others in the literature with regard to morphological appearance, transendothelial electrical resistance, and the permeability coefficient for albumin We then compared our system with in vivo endothelium by studying the movement of neutral and negatively charged radiolabeled dextran tracers across the monolayer and by using electron microscopy to follow the pathways taken by native ferritin. There were a number of differences. The permeability of our monolayer was 10–100 times greater than seen in intact endothelium, there was no evidence of "restricted" diffusion or charge selectivity, and ferritin was able to move freely into the subendothelial space. The reason for these differences appeared to be small (0.5–2.0 μm) gaps between 5 and 10% of the endothelial cells. Although the current use of cultured endothelial cells on porous supports may provide useful information about the interaction of macromolecules with the endothelium, there appear to be differences in the transendothelial permeability characteristics of these models and in vivo blood vessels.

endothelium; albumin transport

REGULATION OF THE MOVEMENT of water and solutes from the vascular to the extravascular space is one of the most important functions of the endothelium. Traditionally, studies of vascular permeability have employed intact animals or isolated-perfused organ preparations. However, with the current ability to grow endothelial cells in culture, a new approach to the study of permeability has become possible using cultured endothelial cells on porous supports.

A number of investigators have successfully grown endothelial cells from a variety of vascular sites and species on suitably treated porous supports to create in vitro models of permeability (2, 9, 10, 12, 18, 24–27, 29). The transendothelial movement of a number of macromolecules has been measured and appears to increase when cells are perturbed by agents such as calcium chelators (25), thrombin (10), or activated leukocytes (12).

The relevance of these observations to the in vivo situation remains unclear. Although the electrical resistance across these endothelial monolayers is low (usually $<20\ \Omega \cdot cm^2$), these values are similar to those measured across frog mesenteric capillaries (7) However, the calculated permeability of larger molecules, such as albumin, across these monolayers is 10–100 times higher than is seen in vivo (10, 25, 26) (see Table 1). The reason for this discrepancy has not been examined. The purposes of this report are to more fully characterize the permeability characteristics of an in vitro endothelial cell-filter system that is similar to that used by others and to determine some of the reasons for the higher permeability to macromolecules that these models show compared with natural endothelia.

To accomplish this, we grew endothelial cells on porous supports and confirmed that our system was similar to others reported in the literature with regard to morphological appearance, transendothelial electrical resistance, and the permeability coefficient for radiolabeled albumin. The endothelial monolayers were then characterized using morphological and physiological techniques that had been used by others in the study of in vivo permeability. The junctional anatomy of our monolayers and the pathways taken by a large electron-dense tracer, native ferritin, were examined using electron microscopy. The rate of movement and pattern of distribution of neutral and negatively charged radiolabeled dextran tracers across the endothelial cell monolayer were also studied.

We found that the permeability of our monolayer to macromolecules was 10–100 times higher than seen in continuous endothelium There was no evidence of charge selectivity. Although large macromolecules moved more slowly across the barrier than smaller ones, these changes could be explained by the differences in diffusion coefficients; i.e., there was no evidence of "restricted" diffusion through pores. In our system, one reason for this increased permeability appeared to be small intermittent gaps between endothelial cells that allowed the leakage of large molecules.

TABLE 1. *Comparisons of permeability to albumin and transendothelial electrical resistance from various EC-filter systems*

| Investigator | Permeability Coefficient for Albumin, cm/s × $10^{-6}$ | Transendothelial Resistance, Ω·cm² | Filter System Characteristics |
|---|---|---|---|
| Shasby & Shasby (25) | 7.7 | 6.1 | Porcine pulmonary artery EC on gelatin/fibronectin-coated Nucleopore filter |
| Garcia et al. (10) | 4.8 | | Bovine pulmonary artery EC on gelatin-coated Nucleopore filters |
| Siflinger-Birnboim et al. (26) | 6.6 | | Bovine pulmonary artery EC on gelatin-coated Nucleopore filters |
| Navab et al. (18) | | 14 | Rabbit aortic EC on gelatin-coated Nucleopore filters |
| Territo et al. (29) | | 15 | Bovine aortic EC on gelatin-coated Nucleopore filters |
| Furie et al. (9) | | 69 | Bovine microvascular EC on treated amniotic membrane |
| Current study | 5.6 | 20 | Bovine fetal aortic EC on fibronectin-coated Nucleopore filters |

EC, endothelial cell.

Although the current use of cultured endothelial cells on porous supports may provide useful information about the interaction of macromolecules with endothelium, there appear to be some important differences between the transendothelial permeability characteristics of our model and in vivo blood vessels.

## METHODS

### *Cell Culture*

A wide variety of endothelial cell lines have been used to prepare in vitro permeability models. To limit the phenotypic variability in our cells, we used a clonal strain of fetal bovine aortic endothelial cells that has been extensively characterized by our laboratory (21, 22). This strain (BFA-39b), labeled AG-7681, is available from the Cell Repository at the Coriell Institute for Medical Research (Copewood Street, Camden, NJ). These cells have been shown to stain positively for factor VIII-related antigen, to exhibit angiotensin I-converting enzyme activity, to take up diacetylated low-density lipoproteins, and to be mycoplasma and virus free. Strain BFA-39b has a well-defined life-span of ~90 population doublings (the equivalent of ~30 passages using 1:3 cell splits) and maintains normal morphology, a constant cellular saturation density, uniform size, as well as producing significant amounts of angiotensin-converting enzyme activity until the 60th population doubling. Cells were used before they had achieved 50 population doublings [i.e., <60% of their expected in vitro life-span (21)]. Cultures were incubated in Ham's F-12 medium supplemented with 20% fetal bovine serum (pretreated at 56°C for 1 h) and an additional 2 mM L-glutamine at 37°C in a 95% air-5% $CO_2$ humidified atmosphere.

For comparison, we also studied the permeability characteristics of a renal epithelial cell line (LLC-$PK_1$, the generous gift of Dr. James Mullin, Lankenau Hospital, Philadelphia). These cells were grown in α-modified Eagle's medium (17) under the identical conditions as the endothelial cells. When mounted on a collagen-coated filter, they formed tight monolayers with a transcellular resistance of ~400 Ω·cm² and a spontaneous transcellular voltage gradient of ~1 mV (17). These measurements on filters seeded with epithelial cells suggest that the filter-ring system used by us allows some types of cultured cells to form tight monolayers.

### *Filter Preparation*

To decrease the chance of edge artifact or disruption of the cellular monolayers by handling, we grew the endothelial and epithelial cells directly on filters previously glued onto plastic rings. Polycarbonate filters (0.8-μm pore diameter, 35-mm filter diameter) were purchased from Nucleopore (Pleasanton, CA) and used for all permeability experiments. Initial use of 3-μm-pore diameter filters was abandoned after microscopy revealed that cells were able to move through these pores and adhere to the underside of the filter after a number of days. The filters were glued onto Lexan plastic rings (25 mm ID, 32 mm OD, 13 mm in depth, 5 cm² area) using nontoxic silicone rubber glue (RTV 118, General Electric, Waterford, NY), allowed to dry overnight, and autoclaved. To facilitate cell adhesion, the filters were treated with bovine fibronectin (Sigma, St. Louis, MO) dissolved in phosphate-buffered saline (PBS) at 25 μg/ml. Two milliliters of this solution were added to the inside of the filter-ring (10 μg/cm²) and incubated for 3 h at 37°C The fibronectin solution was aspirated, and each filter-ring then was seeded with endothelial cells at the supraconfluent density of 3 × $10^5$ cells/cm² (1.5 × $10^6$ cells/filter). Medium was changed the day after seeding and then every 4–5 days. On the day of an experiment, the filter-ring was transferred to the testing chamber (see below).

The LLC-$PK_1$ cells were seeded onto 0.8-μm-pore size polycarbonate filter-rings that had been coated with collagen and sterilized with ultraviolet light. Cells were seeded at 3.6 × $10^5$ cells/cm² and used in permeability experiments 3 days after seeding (17).

### *Staining Procedures*

Since cells grown on the polycarbonate filters used for permeability studies (0.8-μm pore size) were not easily visible using phase-contrast microscopy, we routinely fixed and stained replicate filter-rings before each experiment as well as staining the filter-rings used in each study after the experiment to ascertain the integrity of the monolayer. The filter-rings were washed twice with PBS, fixed in 95% ethanol for 10 min, washed once with distilled water, stained with Gill hematoxylin for 2 min, and washed once with ethanol. The filter was then cut out of the ring with a scalpel blade and mounted.

To visualize cells at the edge of the filter and to demonstrate cell border silver staining directly on polycarbonate filters, we grew cells on fibronectin-coated filters with 3-μm pore diameters (which are more transparent), as described above. After 7 days in culture, the cells were washed with 5% dextrose, treated with 0.4% silver nitrate for 20 min, washed once with 5% dextrose, treated with a 1:1 mixture of 3% cobalt bromide and 1% ammonium bromide for 5 min, washed with 5% dextrose, cut from the ring, and mounted (21).

### *Electron Microscopy*

Endothelial cell-covered filters were routinely prepared in groups of 10–18. We studied at least one cell-covered filter by electron microscopy from six different batches of filter-rings. In addition, four other endothelial-covered filters were studied by electron microscopy after incubation with native ferritin probe.

For these structural studies, monolayers growing on filter-rings were washed twice in PBS and fixed in a mixture of 2.5% glutaraldehyde and 1% osmium tetroxide in 0.1 M cacodylate buffer. The filters were removed from the rings, counterstained with 1% uranyl acetate in maleate buffer, dehydrated, and embedded in epoxy. Thin sections of 700-Å width were cut and photographed in a JEOL 100S electron microscope.

To directly visualize the pathways taken by larger macromolecules through the cell-filter preparation, we utilized native ferritin. Ferritin (type I, Sigma) was dissolved in tissue culture medium at 33 mg/ml and added to the inside of the cell-filter rings. After 5 min incubation, at either 37 or 4°C, the ferritin solution was aspirated and the rings were processed for electron microscopy as described above. Some filters were then counterstained with uranyl acetate while others were processed unstained.

### *Electrical Resistance*

The electrical resistance of the endothelial cell-filter preparation was measured using standard electrophysiological techniques. Rings with surface areas of 2.83 $cm^2$ were used for these experimental studies. Cells were continuously bathed in tissue culture medium (with serum), and the solution was connected to calomel half-cells by 3 M KCl-agar bridges brought to within 0.5 cm of the outer and inner cell surface. Transendothelial current was applied using AgCl-coated silver wires, submerged in a saturated KCl solution, and again connected to the bathing medium via 3 M KCl-agar bridges. By use of a voltage-current clamp apparatus, a current equal to 10 mV was applied across the cell-filter preparation. The resultant change in transendothelial current was used to calculate the total tissue resistance. The electrical resistances of the bathing medium alone and of the filter plus solution were determined and subtracted from the total electrical resistance. The resistance was normalized by surface area and is thus reported in ohms times centimeters squared.

### *Preparation of Dextran Probes*

For permeability studies, we prepared two tritiated polydisperse dextran probes. One probe, the neutral dextran, contained no charge, whereas a carboxydextran probe was negatively charged at physiological pH. We chose to use dextran probes for a number of reasons: *1*) we (16) and others (4, 30) have successfully used these probes for in vivo studies of permeability; *2*) their availability as a polydisperse mixture of molecular sizes makes it possible to investigate a range of effective molecular radii during a single experiment; and *3*) the permeability characteristics of dextran molecules of equivalent sizes, but with different electrical charges, can be compared easily.

The neutral tritiated polydisperse dextran probe used (sp act 113 μCi/mg) was prepared as previously described in detail (16). Briefly, 200 mg of Dextran T500 (Pharmacia Fine Chemicals, Piscataway, NJ) was treated with 1 ml of sodium metaperiodate at 105 mg/ml for 3.5 h followed by reduction with 10–15 mCi sodium borotritiide.

The polydisperse carboxydextran probe was prepared from a tritium-labeled neutral dextran. Fifty to 75 mg of the radiolabeled dextran were dissolved in 2–3 ml $H_2O$, placed in an ice bath, and 1.5 ml of 10 N sodium hydroxide were slowly added while being stirred. After 15 min, the sample was removed from the ice bath and stirred for an additional 10 min. Monochloroacetic acid (1.45 g in 2.5 ml $H_2O$) was added with continual stirring. The solution was placed in an oven at 60–65°C and stirred for 90 min. After removal, the sample was placed in an ice bath, adjusted to pH 5 with glacial acetic acid, treated with 3 vol of ethanol, and left at 4°C overnight. The precipitate was collected by centrifugation, dissolved in 10 ml $H_2O$, and lyophilized. There was no significant loss of radioactivity during this procedure. The carboxydextran probe used in these experiments had a specific activity of 100 μCi/mg.

To establish the charge of the probes, 20,000 cpm of each type were subjected to cellulose acetate electrophoresis at pH 8.6 in 0.075 M barbiturate buffer for 25 min at 250 V. Glycosaminoglycans (polyanions) were applied as markers and stained with alcian blue. Fourteen portions of each electrophorogram from the origin toward the anode through the glycosaminoglycan area were cut and analyzed for radioactivity. Under these conditions, uncharged dextran remained at the origin and carboxydextran migrated toward the anode in the area of hyaluronic acid, a carboxylated polyanion.

The distribution of apparent molecular sizes of the dextran probes after their preparation was determined by molecular sieve chromatography using columns of Sephacryl S-300 (Pharmacia Fine Chemicals) (16). Columns were calibrated using blue dextran and a series of globular proteins with molecular radii of 1.65–8.6 nm. Samples were applied in 2 ml of buffer and collected in 24–26 fractions of 1.6 ml. From each fraction, a 1.0-ml aliquot was added to 5.0 ml liquid scintillation fluid and counted in a liquid scintillation counter (minimum of 4,000 counts).

The distribution of the molecular sizes of dextrans in our neutral polydisperse probe is shown in Fig. 1. The average size was between 4.0 and 5.5 nm. The size distribution of the polydisperse carboxydextran was similar

In some studies, 3 μg/ml of radioactively labeled $^{14}C$-methylated bovine serum albumin (New England Nuclear, Boston, MA; sp act 0.02 mCi/mg) was added in addition to the tritiated dextran probes, and both tracers assayed simultaneously.

*Permeability Studies*

Permeability studies were carried out by placing each filter-ring (32 mm OD) into a 50-ml beaker (38 mm ID). The filter-ring rested on top of a plastic stand (3 mm high) that allowed free flow of fluid under and around the ring. The addition of 2.5 ml of medium to the inside of the filter-ring ("top chamber") and 7.0 ml of medium outside the ring in the beaker ("bottom chamber") resulted in equal fluid levels within and outside the ring and thus prevented any hydrostatic pressure gradients across the filter. All experiments were performed with tracers dissolved in tissue culture medium (Ham's F-12) supplemented with 20% fetal bovine serum. A pH of ~7.4 was maintained by placing the beakers (covered to prevent evaporative losses) inside an incubator at 37°C in a humidified, 5% $CO_2$ atmosphere. To minimize the effect of unstirred layers, we placed the beakers containing rings on an orbital shaker operating at ~60 rev/minute.

After a 1-h equilibration, the medium inside each ring (top chamber) was replaced with media containing labeled probe. Fifty-microliter samples of medium from the lower chamber were obtained at various times for determination of total counts of radioactivity that had traversed the filter. After 4.5 h, the molecular size distribution of the polydisperse probe in each chamber was determined by placing aliquots on a molecular sieving column as described above. The ratio of counts in the bottom chamber to counts in the top chamber for each of the 24 column fractions was calculated, thus enabling us to plot a distribution of bottom-to-top ratios vs. molecular size for dextrans with molecular radii of 1.6–9.6 nm. It was thus possible to directly compare the permeability characteristics of charged vs. uncharged dextrans of equivalent molecular radii.

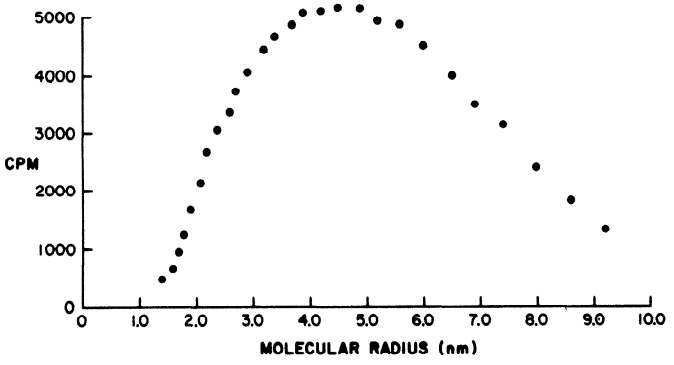


FIG. 1. Molecular size distribution of tritiated polydisperse neutral dextran probe. An aliquot of probe was applied to a precalibrated Sephacryl S-300 column, and radioactivity in each fraction was determined. Counts per minute detected in each fraction were plotted against effective molecular radius (nm) of probe.

We also wanted to determine the contribution of the subcellular matrix produced by the endothelial cells to the restriction of macromolecular movements. This was accomplished by treating six endothelial cell-covered filters (that had been used in the aforementioned permeability experiments) with the nonionic detergent Triton X-100 (0.5% vol/vol in PBS) for 30 min, followed by two gentle washes. This treatment effectively removes the cell layer while leaving the subcellular matrix intact (11). The amount of neutral and carboxydextran probes that moved across these Triton-treated filters over 1 h was measured and compared with the results of the endothelial-covered filters and the unseeded fibronectin-coated filters.

*Calculation of Permeability*

To standardize our results and to allow comparisons with in vivo data and the results of other in vitro experiments, we calculated the permeability coefficients for dextrans of various sizes and of albumin in the following manner from an approximation of Fick's law

$$J = AD\frac{\Delta c}{\Delta x} \quad (1)$$

where $J$ is the flux of molecules across the filter expressed as counts per second, $A$ is the surface area available for diffusion (calculated as 5 $cm^2$ in our system), $D$ is the diffusivity of the probe, $\Delta x$ is the thickness of the barrier, and $\Delta c$ is the concentration difference between chambers. Although the concentration difference changed over the course of the experiment, the total amount of probe crossing the monolayer and filter was sufficiently small (<10% for most sized probes) to allow us to estimate $\Delta c$ by the concentration of tracer in the top chamber ($C_T$) minus the concentration of tracer in the bottom chamber ($C_B$) or

$$\Delta c = C_T - C_B \quad (2)$$

By definition, the permeability coefficient ($P$) equals $D/\Delta x$ or

$$P = D/\Delta x \quad (3)$$

Substitution of *Eqs. 2* and *3* into *Eq. 1* leads to

$$P = J \cdot 1/A \cdot 1/(C_T - C_B) \quad (4)$$

P can thus be calculated, since each variable on the right side of *Eq. 4* can be defined experimentally. Mathematical corrections for unstirred layer effects were not made because application of the results of Barry and Diamond (1) shows that the measured permeability overestimates the actual membrane permeability by <10%.

In addition to the calculation of permeability coefficients, the distribution of bottom chamber-to-top chamber ratios allowed us to analyze our results in a manner similar to that used in studies of lymph-to-plasma ratios obtained from intact-animal studies (16, 25, 28). We specifically sought to determine whether the movement of dextrans between the chambers could be used to

characterize the dextran pathway through our monolayers. The following assumptions were made: *1*) that the tracer was not metabolized and the total amount remained constant over the time course of our experiments; *2*) that the amount of tracer within the filter and cell layer at any measurement time was negligible (this assumption was supported by directly measuring the total counts added at the beginning of an experiment and the total counts recovered at the end of an experiment); and *3*) that transport between the chambers occurred entirely by a diffusive process which obeyed Fick's law of diffusion. With these assumptions, the expression for the ratio of tracer between the two chambers as a function of the incubation time ($t$) is given by

$$\frac{C_B}{C_T} = \frac{1 - \exp\left\{-\frac{AD}{\Delta x}\left(\frac{1}{V_T} + \frac{1}{V_B}\right)t\right\}}{1 + \frac{V_T}{V_B}\exp\left\{-\frac{AD}{\Delta x}\left(\frac{1}{V_T} + \frac{1}{V_B}\right)t\right\}} \quad (5)$$

where $V_T$ and $V_B$ are the volumes of the top and bottom chambers. Because of the dependence of $\Delta x$, $A$, and $D$ on the tracer size and pathway geometry, it is possible to determine whether there is interaction of the tracers with the transport pathway. By use of the simplest possible model, that of a system of cylindrical pores of a single size, free diffusion of macromolecules will be impeded if the tracer size is similar to the pore size. This restriction to free diffusion can be mathematically described as a function of the ratio of the tracer radius to pore radius ($a/r$) and one other unknown that represents the total pore area divided by the characteristic pore length ($A_{pores}/\Delta x$). This expression has been used extensively by others (25, 28) and is given by

$$\frac{AD}{\Delta x} = D_{free}\cdot\frac{A_{pores}}{\Delta x}\cdot\left(1 - \frac{a}{r}\right)^2\cdot\left[1 - 2.104\left(\frac{a}{r}\right) + 2.09\left(\frac{a}{r}\right)^3 - 0.95\left(\frac{a}{r}\right)^5\right] \quad (6)$$

In this expression, $D_{free}$ is the free diffusion coefficient of each dextran tracer and was computed from the Stokes-Einstein equation

$$D_{free} = \frac{kT}{6\pi a\eta} \quad (7)$$

where $T = 313°K$, $k$ is the Boltzmann constant $= 1.38 \times 10^{-16}$ g·cm$^2$·s$^{-2}$·°K$^{-1}$, $\eta$ is solvent viscosity $= 6.7 \times 10^{-3}$ g·cm$^{-1}$·s$^{-1}$, and $a$ is the tracer radius.

To model our experimental data, we created a computer program that allowed us to pick empirical values for the equivalent pore radius ($r$) and the total pore area divided by the pore length ($A_{pores}/\Delta x$) and that used *Eqs. 5–7* to generate concentration ratios ($C_B/C_T$) for each sized dextran. We then compared these calculated tracer ratios with the experimental data and adjusted the model parameters ($r$ and $A_{pores}/\Delta x$) to minimize the sum of squared differences.

## RESULTS

### *Morphology of Endothelial Monolayers*

When stained with hematoxylin, the endothelial cell-covered filters showed a confluent layer of cells (Fig. 2). The cells had an elongated shape for the first 2–3 days after seeding but then assumed the more characteristic cuboidal configuration. After 7 days in culture, positive silver staining at cell borders was present (Fig. 2). An intact layer of endothelial cells was visualized all the way to the edge of the filter. The cells, in fact, grew over the top of the silicone glue that sealed the plastic ring to the polycarbonate filters.

Electron microscopy of seeded filters revealed a continuous layer of flattened endothelial cells that appeared similar to the endothelial cells seen lining large vessels in vivo and exhibited a variety of junctional types including end-to-end (Fig. 3*A*), simple overlap (Fig. 3*B*), mortise, and complex (Fig. 3*C*) (23). Many of these junctions had areas of membrane fusion (Figs. 3*C* and 9) characteristic of the "tight junctions" seen in vivo (13). While most endothelial cell junctions appeared similar to those seen in vivo, when large numbers of cell junctions were counted, approximately five to ten percent of the intercellular borders were discontinuous with gaps of approximately 0.5–2 μm between cells (Fig. 3*D*).

A subcellular matrix material was produced by the cells which increased in thickness as the time in culture increased (Fig. 3). Occasionally, "sprouting" endothelial

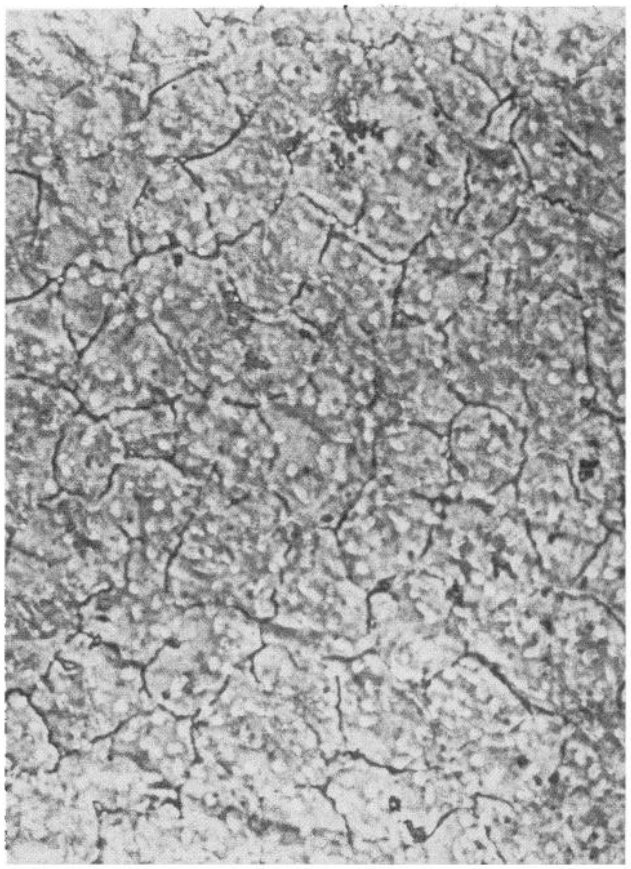

FIG. 2. Light micrograph of endothelial cells on a fibronectin-coated filter with cell borders stained with silver nitrate (×380).

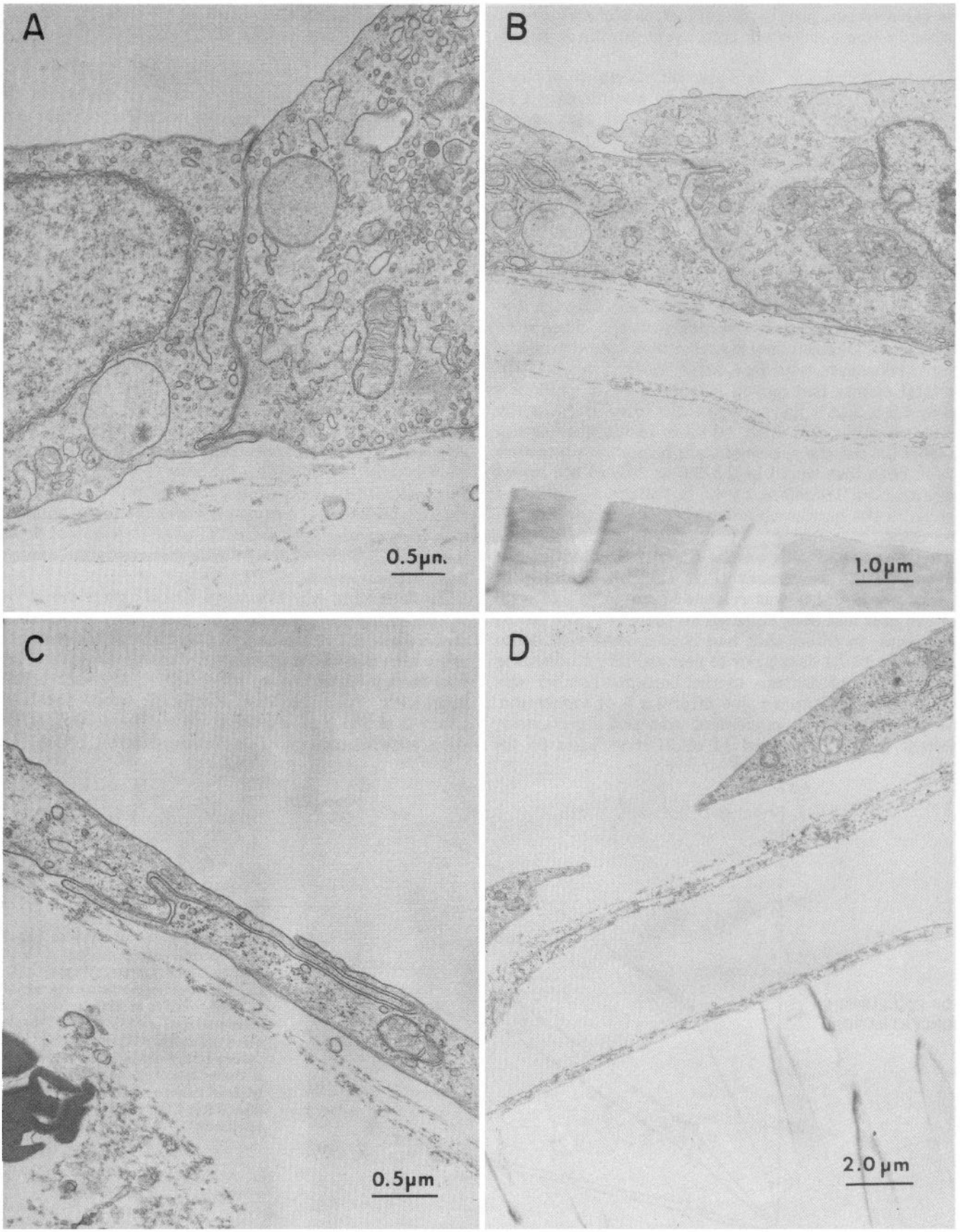


FIG. 3. Electron micrographs of endothelial cells grown on fibronectin-coated Nucleopore filters for 14 days. A variety of junctional structures are present—*A*: "end-to-end" (×20,000); *B*: "simple overlap" (×10,800); *C*: "complex" (×24,000); *D*: "discontinuous" (×6,300).

cells appeared beneath the monolayer, as is characteristic of some bovine endothelial cultures at confluent densities.

*Electrical resistance.* The electrical resistance of three filters covered with endothelial cells was measured 14 days after seeding. The resistance of the cells plus matrix totaled 36 $\Omega \cdot cm^2$; after treatment with Triton-X 100 (to lyse the cellular layer), the resistance was 16 $\Omega \cdot cm^2$. The resistance of the matrix was therefore 16 $\Omega \cdot cm^2$, and the cellular contribution to electrical resistance was 20 $\Omega$ $cm^2$.

*Permeability Studies*

The rate of neutral dextran movement through the filter system was initially measured in the absence of cells (Fig. 4). Dextran moved across unseeded filters in a manner consistent with free diffusion. By 1 h, 12.4% of the total counts had moved into the bottom chamber, and by 4.5 h, 22.8% had traversed the filter. Because the bottom chamber contained 7.0 ml of media and the top chamber 2.5 ml, the expected equilibrium concentration of both chambers would be 2.5/9.5 or 26% of the initial concentration. Therefore, by 4.5 h, the concentration of dextran in the bottom chamber was 77% of the equilibrium value.

The presence of cells on the filter clearly slowed the rate of dextran movement (Fig. 4). This decrease in dextran permeability was related to the length of time that the cells had been cultured on the filter prior to the experiment. In filters that had been seeded with endothelial cells 14–21 days prior to permeability studies, the concentration of dextran in the bottom chamber was 19% of the equilibrium value after 4.5 h of incubation. The rate of dextran movement was not significantly different for filters seeded 14 or 21 days prior to the experiment (Fig. 4), and therefore all experiments were performed on filters seeded with cells 14–21 days previously.

The distribution of dextran fractions after 4.5 h of equilibration, expressed as the ratio of counts in the bottom chamber to top chamber vs. the molecular size, is illustrated in Fig. 5 for a typical endothelial monolayer and an LLC-$PK_1$ epithelial monolayer. For the polydisperse neutral probe, dextrans of smaller size moved into the bottom chamber at a faster rate than did dextrans of larger size. As might be expected from in vivo measurements (6), the epithelial monolayer was less permeable to dextrans than the endothelial monolayer. However, the pattern of restriction was quite different; the epithelial layer restricted the passage of smaller dextrans to a much larger degree than did the endothelial layer. For example, for a dextran of molecular radius 3.9 nm (the size of methylated albumin), the ratio of counts in the bottom chamber to that of the top chamber was 0.063 for the endothelial layer vs. 0.034 for the epithelial layer (a 2-fold difference), whereas for a dextran of molecular radius 1.4 nm the ratio was 0.28 for the endothelial layer vs. only 0.047 for the epithelial layer (a 6-fold difference). The calculated permeability coefficients for dextrans through endothelial monolayers over the range of molecular sizes examined and for $^{14}C$-methylated albumin are tabulated in Table 2. Each value represents the mean of five determinations

To determine whether there was a charge selectivity to this pattern of dextran movement, we compared the movements of the uncharged polydisperse tritiated dextrans with that of the polydisperse tritiated dextrans that had been modified to be negatively charged at pH 7.4 and with $^{14}C$-methylated albumin (also negatively charged at pH 7.4). Figure 6 shows the results of five such experiments using a carboxydextran probe. The

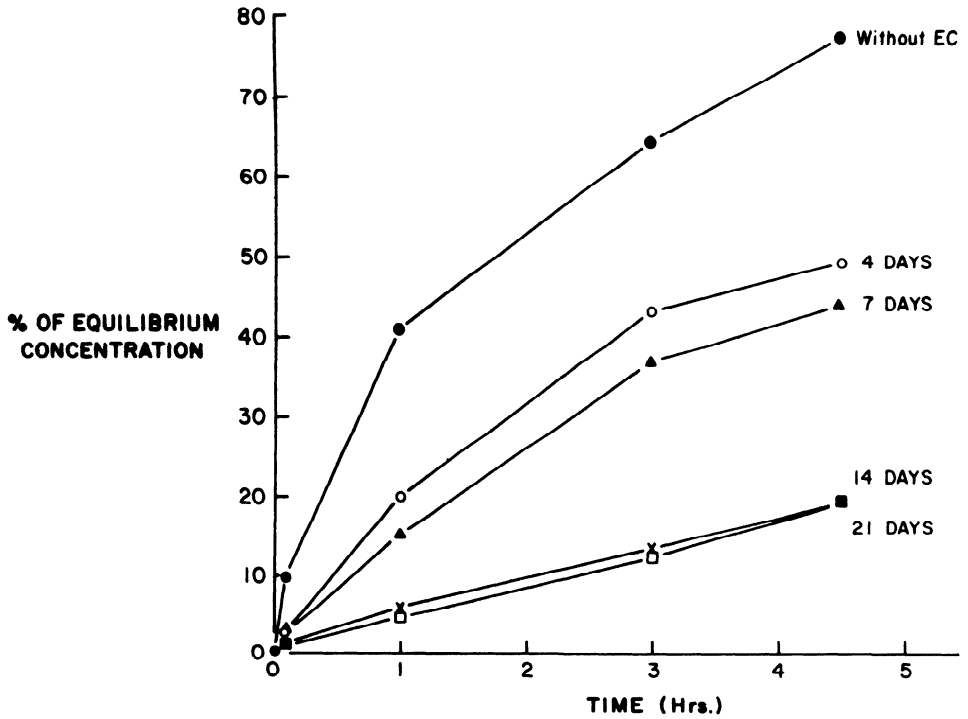


FIG. 4. Passage of tritiated polydisperse neutral dextran through filter-ring system. Concentration of tracer in bottom chamber (expressed as a percentage of final equilibrium concentration) was measured over a 4.5-h period. Three filters were coated with fibronectin but not seeded with endothelial cells (●). Other fibronectin-coated filters were seeded with endothelial cells (EC) and tested after 4 (○), 7 (▲), 14 (×), and 21 (□) days in culture.

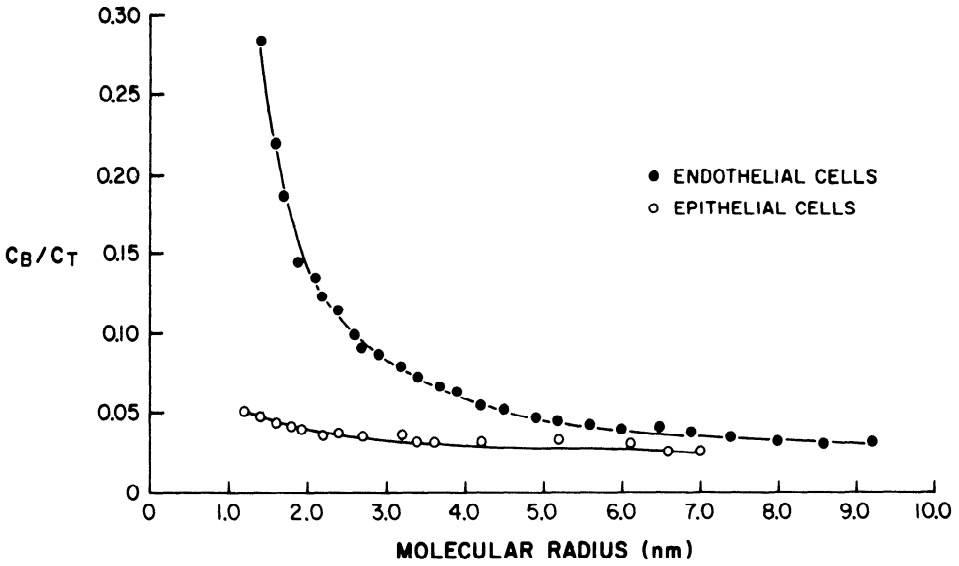


FIG. 5. Distribution of tritiated polydisperse neutral dextrans across a typical endothelial cell-covered filter and an epithelial cell-covered filter after 4.5 h of incubation. Ratio of counts in bottom chamber to top chamber ($C_B/C_T$) is plotted against molecular radius (nm) for each dextran fraction. A ratio of 1.00 for $C_B/C_T$ represents complete equilibration between bottom and top chambers.

TABLE 2. *Permeability coefficients of dextrans and albumin measured in vitro and in selective organ systems*

| Tracer | Molecular Radius, nm | Permeability Coefficients, cm/s × $10^{-6}$ | | | | | |
|---|---|---|---|---|---|---|---|
| | | In vitro* (current study) | In vitro† (Ref. 26) | Dog paw | Dog intestine | Dog heart | Sheep lung‡ |
| Dextrans | 1.6 | | 120 | | | | |
| | 2.2 | 13.9 | | | | | 0.1 |
| | 2.4 | 12.3 | | | | | 0.08 |
| | 2.8 | 8.8 | 20 | 0.3 | 0.3 | | 0.05 |
| | 3.6 | | 6.6 | 0.08 | 0.07 | | 0.03 |
| | 4.0 | 6.1 | | 0.04 | 0.03 | | |
| | 4.5 | | 3.3 | | | | |
| | 5.2 | 4.5 | | 0.01 | 0.005 | 0.007 | |
| | 6.0 | 3.9 | | 0.005 | 0.003 | 0.003 | 0.01 |
| | 7.0 | 3.3 | | | | 0.004 | 0.008 |
| | 8.0 | 3.0 | | | | 0.004 | 0.006 |
| | 9.0 | 2.7 | | | | 0.004 | 0.004 |
| | 10.6 | | 1.2 | | | | |
| Albumin | 3.9 | 5.6 | 6.6 | 0.047 | 0.029 | 0.029 | 0.014 |

Adapted from Table 3 of Ref. 20. * Each value represents the mean of 5 separate determinations and was calculated as described in METHODS. † A variety of $^{125}I$-labeled proteins used (see Ref. 26). ‡ Molecular tracer used was polyvinylpyrrolidone instead of dextran.

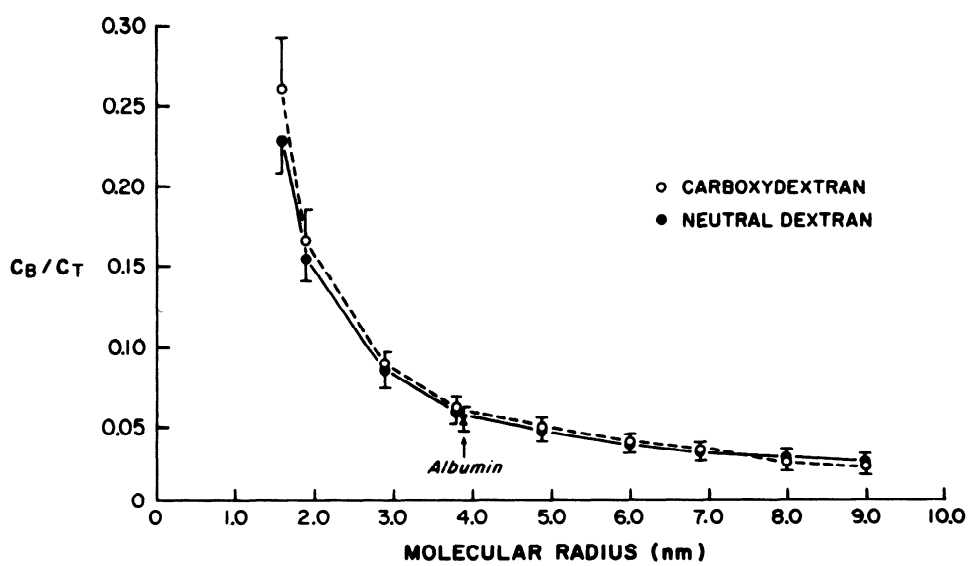


FIG. 6. Distribution of tritiated dextrans and $^{14}C$-labeled methylated albumin across endothelial cell-covered filters after 4.5 h of incubation. Ratio of counts in bottom chamber to top chamber ($C_B/C_T$) is plotted against molecular radius (nm) of 9 fractions of neutral dextran and negatively charged carboxydextran. In addition, $C_B/C_T$ of $^{14}C$-methylated albumin is shown (↑) as a function of its molecular size. Values represent mean ± SE of 5 determinations.

pattern of permeability was identical for neutral dextran and carboxydextran. The movement of methylated albumin closely followed that of neutral and carboxydextran. Thus there was no evidence of charge selectivity in this system.

The relative contributions of filter, matrix, and endothelial cells to the restriction of neutral and carboxydextran movement is shown in Fig. 7. The endothelial layer was the primary barrier to dextran movement. The presence of an intact endothelial cell layer over the matrix impeded the movement of dextrans 85% more than control conditions. Less than half of this effect was due to the subcellular matrix, which restricted dextran movement only by ~35% more than control. There was no difference in the movement of neutral or negatively charged dextrans through the matrix, thus no evidence of charge selectivity.

The pattern of dextran distribution indicates that larger dextrans moved across the endothelial barrier at a slower rate than smaller molecules, consistent with the proportionality of diffusion to molecular size. We used our computational model to determine whether this pattern reflected the passive diffusional characteristics of the dextrans (simple diffusion) or whether there was evidence of interaction of the tracers with pores in the membrane (restricted diffusion). By empirically adjusting our estimates of pore radius and pore area/path length ($A_{pores}/\Delta x$) we were able to best-fit our experimental data to the computer-generated predictions by choosing a pore radius of 66 nm and a $A_{pores}/\Delta x$ of 44 cm (Fig.

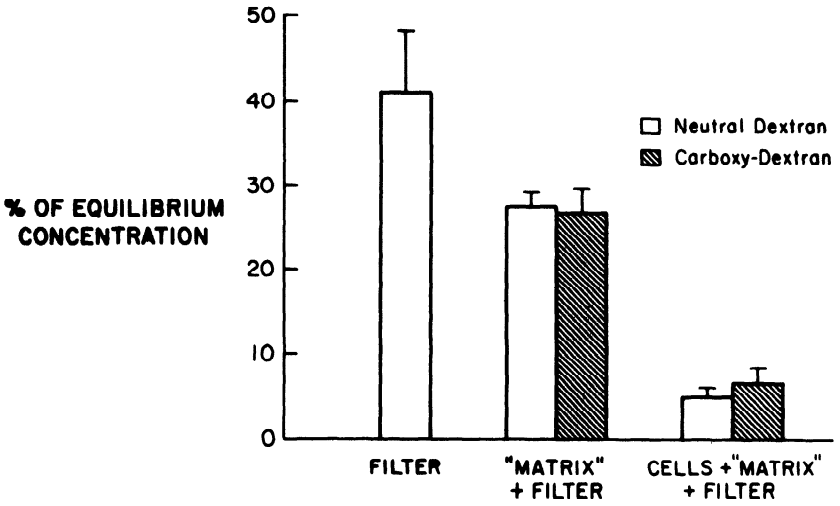


FIG. 7. Passage of tritiated neutral and carboxydextran through filter-ring system. Concentration of tracer in bottom chamber (expressed as a percentage of final equilibrium concentration) was measured after 1 h using fibronectin-coated filters (without cells), fibronectin-coated filters on which endothelial cells had grown for 14 days, and endothelial-cell covered filters that had been treated with Triton X-100 to remove cell layer and expose subcellular matrix.

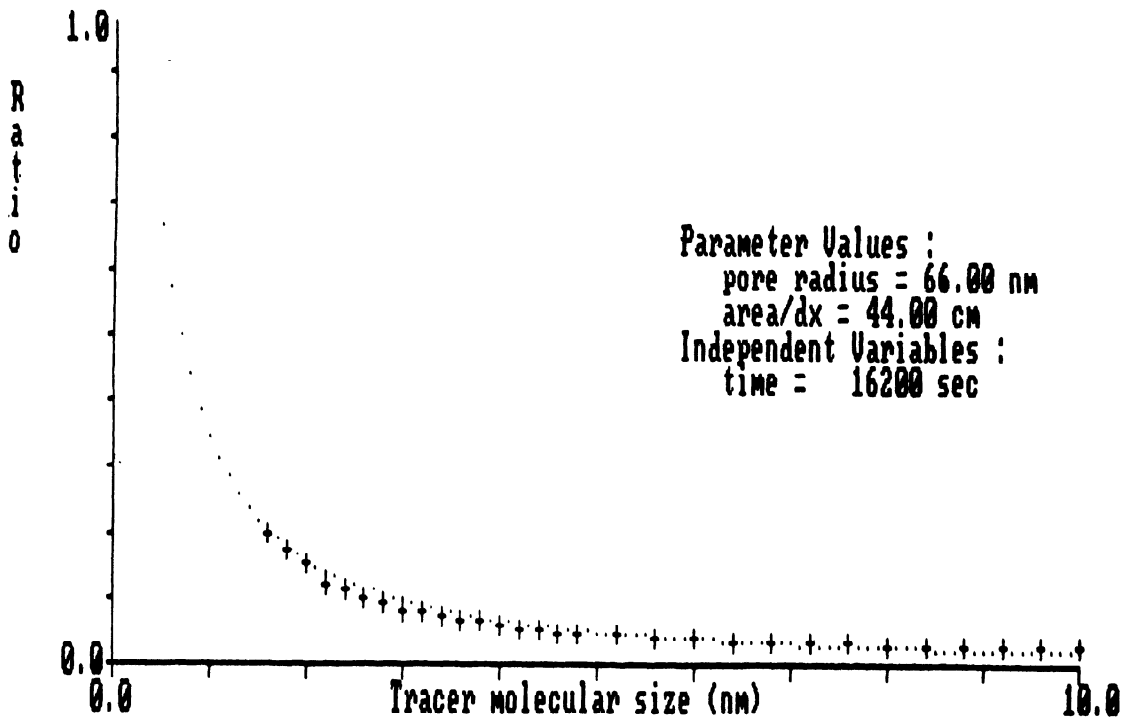


FIG. 8. An experimentally obtained distribution of neutral tritiated dextran probe across endothelial cell covered filters (+) after 4.5 h compared with best-fitting computer-generated data points (·). As in Figs. 5 and 6, ratio of counts in the bottom chamber to top chamber ($C_B/C_T$) is plotted against molecular radius of tracer (nm). Closest fit of experimental data to a 1-pore model was obtained by setting pore radius equal to 66 nm and $A_{pores}/\Delta x$ equal to 44 cm (see text for details).

8). There were, however, only small changes in the computer-generated data points when larger pore radii were used, suggesting little, if any, interaction of the tracers with pores (i.e., little evidence of restricted diffusion).

*Electron-Microscopic Tracers*

To examine further the transendothelial pathways traversed by tracers in these experiments, we used electron microscopy to follow the movement of native ferritin through endothelial cells on seeded filters. Ferritin has a molecular radius of 6.1 nm, is negatively charged at physiological pH, and therefore is not strongly bound to cell surfaces. A number of studies using ferritin as an in vivo tracer in whole animals or perfused organs have shown that this molecule is not normally detected in cell junctions and presumably passes through the endothelial barrier solely by vesicular transport or through intercellular discontinuities in the endothelial barrier (5, 13, 14).

After 5 min of exposure, at both 4 and 37°C, large amounts of ferritin were detected in the subendothelial matrix (Fig 9). The ferritin was present diffusely, however, larger clumps of aggregated tracer could be seen in the vicinity of the cellular gaps (Fig. 9*C*). At 37°C, a small number of ferritin particles was detected in both coated and uncoated vesicles; however, at 4°C, ferritin was not visualized inside the uncoated vesicles (Fig. 9*B*). Only rare ferritin particles were seen within the intact cell junctions (Fig. 9*A*). It therefore appeared that although a limited amount of ferritin could pass the endothelial barrier via vesicular transport, the primary route for ferritin passing across the endothelial monolayer was through the gaps between cells.

## DISCUSSION

The use of an in vitro model of permeability has a number of advantages, such as offering direct access to luminal and albuminal fluid for analysis, being highly simplified and limited to a single cell type, and having an experimental milieu that can be defined in terms of the chemical composition, pressure, and shear conditions of the incubation medium. However, the very factors that simplify the system also raise questions about its relevance to the intact in vivo situation. All models of in vitro permeability require that the endothelial cells be grown on some sort of artificial substrate, such as gelatin or fibronectin-coated nitrocellulose or polycarbonate filters or treated amniotic membrane. The effect of these substrates on endothelial junctional anatomy is unclear. In addition, the influence of the basement membrane, subcellular matrix region and interstitium on vascular permeability are altered considerably in the in vitro model.

To accurately interpret data obtained from endothelial cell monolayer systems, it is important to understand their detailed permeability characteristics. To date, these models have been analyzed by measuring transendothelial electrical resistance and/or permeability to albumin. Although the electrical resistance has been close to that observed by some investigators in vivo (7), the permeability to albumin has been quite different from that reported in intact-organ preparations (3, 15, 20, 28).

The reasons for the discrepancy between electrical resistance and the increased permeability to macromolecules in these models remain unexplained. It is also unknown whether these monolayers resemble intact endothelia with respect to the presence of restricted diffusion, charge selectivity, or ferritin exclusion. The role of the subcellular matrix produced by the cultured cells has also not been studied.

The purpose of this study was to examine some of these issues. Our model was first compared with those preparations used by others and then characterized using techniques that have been employed previously in intact-animals or -organ physiological experiments.

*Comparisons to Other In Vitro Models*

One problem in comparing data from in vitro monolayer systems has been the different methodologies used by each investigator. A number of types of endothelial cells have been used [porcine pulmonary artery (24, 25), bovine aorta (12, 29), bovine pulmonary artery (10, 26, 27), bovine adrenal cortex microvasculature (9), rabbit aorta (18), and rat brain microvasculature (2)] studied at different passages (ranging from primary to passage 22) at different times after cell seeding, on different substrata, and in different-sized and configured chambers. The quantification of permeability has not been standardized, thus making direct comparisons even more difficult.

Our model system employed a well-characterized line of bovine fetal aortic endothelial cells at a passage level before any evidence of cellular senescense has been detected. The filter surface was modified by coating with fibronectin. In preliminary studies we found no advantage to using collagen alone (either with or without prior treatment of the filter with acid) or collagen plus fibronectin-coated filters. We also found that maximum resistance to macromolecular transport occurred 14 days after cell seeding. Even though we (as has each previous investigator) developed our own experimental preparation, we also carefully compared our system with those reported in the literature (2, 9, 10, 12, 18, 24–27, 29). By light microscopy, the cells formed a continuous-appearing monolayer and the cell borders stained positively with silver nitrate (Fig. 2). The appearance of the intercellular junctions, by electron microscopy, was similar to the descriptions published by others (Fig. 3). Our filters also appeared similar to those of others in terms of two functional parameters, electrical resistance and the permeability to albumin. Table 1 presents a detailed comparison of our system to a number of others. When the permeability coefficient for albumin was not provided, we were able to calculate this value using the equation described in METHODS. The similarities in these parameters among the different models is striking. Thus, by at least these measurable criteria, our system seems comparable to other similar models, although it is possible that subtle methodological differences may be important.

The results of our study should be compared with those of the recent publication by Siflinger-Birnboim et al. (26). These authors studied the molecular sieving characteristics of bovine pulmonary artery endothelial

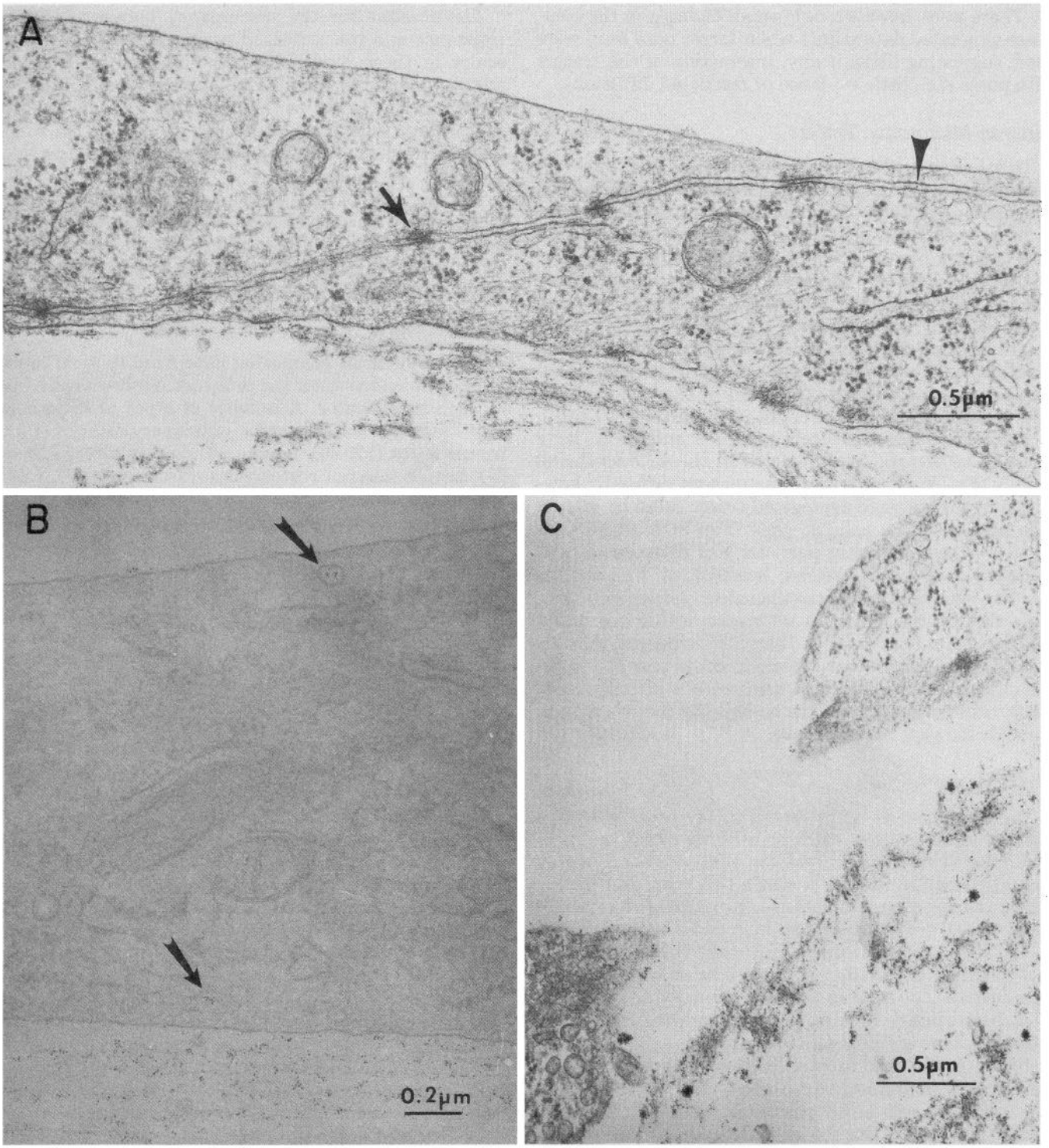


FIG. 9. Electron micrographs of endothelial cells grown on fibronectin-coated Nucleopore filters for 14 days and then exposed to native ferritin for 5 min. *A*: extensive deposits of ferritin can be seen binding to subendothelial matrix material in bottom of photomicrograph. A few particles are seen on luminal surface, and one particle can be seen in cell junction near luminal surface (▼). Areas of membrane fusion or tight junctions (↘) appear to exclude further movement of ferritin particles (×47,000). *B*: an unstained preparation in which ferritin is detectable beneath cell layer as well as within 2 vesicles (↘) (×50,000). *C*: areas of discontinuity between cells that may provide a route for ferritin to traverse the monolayer. Note larger clumps of ferritin appearing at gap (×34,000).

cells on gelatinized filters and concluded that restricted diffusion did occur and that a two-pore model could best explain their results. Despite some methodological and computational differences, a careful examination of their data compared with ours (see Table 2) reveals that the permeability coefficients calculated for the large-size molecules are very similar (e.g., their permeability coefficient for albumin was $6.6 \times 10^{-6}$ cm/s, whereas ours

was $5.6 \times 10^{-6}$ cm/s). The difference in the two sets of data arises from the much larger permeability coefficients that Siflinger-Birnboim et al. obtained for their smaller tracers. Thus, because their monolayer was leakier to small tracers, they concluded that restricted diffusion was occurring. It is unclear at this time what explains this difference in small tracer permeability. Regardless, despite the evidence that their monolayer showed characteristics of restricted diffusion, this system is just as permeable, in fact more permeable, than ours.

*Morphological Characteristics*

*Comparison to in vivo endothelium.* By light microscopy, the endothelial cell layer on the filter appeared similar to the continuous endothelium of large blood vessels. The cells formed an intact monolayer and exhibited the characteristic silver staining of cell borders that is seen between cells that grow in vivo (9).

Electron microscopy of our preparation also revealed several other similarities to continuous endothelial layers. The endothelial cells on the filters appeared flattened and thin and had a normal distribution of cellular organelles. Vesicles were observed (Fig. 9), although at a density less than has been usually described in vivo (5, 13). Most cell junctions appeared similar to those described in large vessels (23) and showed both simple (Fig. 3*A*) and complex (Fig. 3, *B* and *C*) interdigitations. Characteristic tight junctional areas were visible between cells (Fig 9*A*). Interestingly, cultured endothelial cells seeded on filters made a matrix that by electron-microscopic examination resembled the basement membrane produced by the endothelium in vivo. After 2 wk in culture, this layer of matrix was approximately as thick as the cell layer (Fig. 3).

Careful review of a large number of sections, however, revealed at least one important difference between endothelial cells seeded on the filter and those in continuous endothelium. Between 5 and 10% of the cells were not tightly joined but had small gaps (0.5–2 $\mu$m in length) between them (Fig. 3*D*). The fact that large clumps of ferritin particles could only be seen in the vicinity of the cellular gaps (Fig. 9*C*) argues strongly that these openings were present during actual permeability studies and are not artifacts of fixation. If the gaps had been formed by cell retraction or detachment during fixation (after the ferritin had been removed from the monolayer), one would have expected to see a uniform distribution of ferritin particles similar to that visualized under the intact cell layer.

*Permeability Characteristics*

*Morphological observations.* Native ferritin is an electron-dense tracer with a molecular radius of 6.1 nm. It has been used extensively in studies of permeability in vivo (5, 14). This molecule, which is negatively charged at physiological pH, does not bind extensively to cells except at the "coated pit" areas of the membrane (5, 14). In vivo, transport of ferritin across continuous nonfenestrated endothelium is markedly restricted. Little, if any, ferritin traverses intact cell junctions, and most of the transport is thought to be vesicular (5, 14).

In our system, large amounts of ferritin were visualized under the endothelial layer after only 5 min exposure (Fig. 9). This deposition was probably not due to vesicular transport because very few ferritin particles were seen within vesicles during this time, and more importantly, substantial ferritin deposition was still observed at 4°C, at which temperature vesicular transport is negligible. In addition, there was no evidence for ferritin leakage through the intact cell junctions. Only rare ferritin particles could be visualized within cell junctions, and those that were seen were close to the upper cell surface (Fig. 9*A*). On the basis of these observations, it seems likely that the primary site of ferritin transport to the subendothelial matrix was through the intermittent cell gaps.

*Electrical resistance measurements.* The permeability characteristics of in vivo endothelium have been analyzed in a number of ways. One approach has been to measure the electrical resistance to current flow, a modification of the technique used extensively in the study of epithelial cells, both in intact tissues and in culture (6). In contrast to the high resistances (400–1,000 $\Omega \cdot cm^2$) found in these epithelial tissues and in brain epithelium [1,300 $\Omega \cdot cm^2$ (8)], the tissue resistances of intact rabbit aortic endothelium [9.7 $\Omega \cdot cm^2$ (19)] and frog mesenteric capillaries [1.85 $\Omega \cdot cm^2$ (7)] are much lower. These lower electrical resistance measurements are similar to those found in a number of in vitro systems, including our own (Table 1).

The validity of using electrical resistance as a measure of vascular permeability in "nonbrain" endothelia, however, has not been established. Unlike the brain endothelium and most epithelial membranes, where the primary physiological function of the barrier is to restrict water and ionic transport, most endothelial barriers permit relatively free movement of these small molecules to allow equilibration between the vascular and extravascular space. The regulation of solute flux between these compartments is primarily controlled by the Starling forces of hydrostatic and oncotic pressure. Macromolecular permeability (particularly albumin flux) is especially important in maintaining oncotic pressure differentials.

In contrast to the epithelial barrier, where high resistance to both small and large molecules is present, the nonbrain endothelium is characterized by a relatively low resistance to small ion flux (i.e., low electrical resistance) coupled with relatively high resistance to macromolecules. These differences can also be seen in vitro (Fig. 5). The endothelial barrier was six times as permeable to small molecules (1.4-nm molecular radius) as the epithelial barrier, yet only two times as permeable to larger albumin-sized molecules.

It therefore appears that the measurement of electrical resistance may not accurately reflect endothelial macromolecular permeability and thus may not be as useful as it has been in the study of epithelial barriers. Further support for this hypothesis is provided by the study of Navab et al. (18), who showed that permeability to some macromolecules (albumin and low density lipoprotein) could be increased across an endothelial monolayer system without a concomitant increase in transendothelial resistance. We suggest that this may explain the appar-

ent paradox of in vitro endothelial monolayers showing "physiological" levels of electrical resistance while at the same time being much more permeable to albumin (and other macromolecules) than are in vivo endothelial barriers.

*Macromolecular permeability measurements.* An extensive amount of information, much derived from studies of lymph flow and composition, exists about the passage of macromolecules across a variety of capillary beds (20, 28). Renkin (20) has calculated the permeability of capillaries in selected organs to dextrans of various sizes and to albumin by dividing the measured permeability-surface area product by the estimated capillary surface area. These estimates are diffusional permeabilities calculated on the assumption that diffusion or vesicular exchange rather than convection is the dominant mode of transport. To the extent that convective transport is involved, they are overestimates of the true permeabilities. Nonetheless, this tabulation allows a direct comparison of our data with a number of in vivo estimates (Table 2). In general, the permeability coefficients obtained in vivo are at least 100-fold smaller than measured by us in vitro.

Supplementing the data obtained from lymph flow analysis are more direct measurements of albumin passage through endothelium. Joyner and Curry (15), using micropuncture techniques, calculated a permeability coefficient of $2 \times 10^{-7}$ cm/s in hamster mesenteric capillaries perfused with 10 $cmH_2O$ pressure (15). Bratzler et al. (3) calculated the permeability coefficient of radiolabeled albumin to be $4 \times 10^{-8}$ cm/s in intact rabbit aortic endothelium by directly measuring tissue radioactivity over time. Again, these data suggest that the in vitro model is 10- to 100-fold more permeable than intact continuous endothelium.

In addition to direct comparisons of permeability coefficients, the pattern of macromolecular movement through the endothelial barrier can be analyzed. Data obtained from in vivo experiments have shown that the movement of large macromolecules across endothelial barriers is impeded to an extent greater than can be explained by simple diffusion. The concept of restricted diffusion or "molecular sieving" has thus been proposed; this model assumes an interaction between macromolecules and at least two sets of "pores"; a large number of small pores of radius 5–8 nm and a smaller number of large pores, 20–25 nm in radius (28).

In this context, the pattern of permeability in our system can be compared with that seen in vivo. Although it would be possible to fit a two-, three-, or more pore model to our results, our data could be closely modeled by a simple one-pore model with a very large pore radius of 66 nm (Fig. 8). The "closeness of fit" was in fact changed very little by increasing the pore size up to 200 nm. The large difference between the calculated pore size and the largest tracers used (up to 9 nm) and the insensitivity of the model to increasing pore size indicates that there was little evidence of interaction between tracer and pores and therefore little restriction to free diffusion. This result suggests that there are either no "small-pore" restriction pathways present or that this method is not sensitive enough to detect a small fraction of the tracers passing through restricted pathways in combination with most of the tracer passing through large unrestricted pathways (which could include gaps between cells or possibly transcytotic paths).

In addition to size selectivity of intact endothelium, a growing body of information suggests that a charge selectivity also exists. As examples, the movement of negatively charged dextrans across the renal endothelial layer is much slower than that of neutral or positively charged dextrans (4). In an intact nephrectomized rat model, $^{125}$I-labeled albumin (negatively charged) remained confined to the vascular space for a much longer time than did $^{14}$C-labeled neutral dextran of comparable size (30). In contrast, we found no evidence of charge selectivity in our intact endothelial-covered filter or in the endothelial matrix-covered filter. There were no differences in the permeability coefficients of neutral dextrans, negatively charged dextrans (carboxydextran), or $^{14}$C-methylated albumin molecules (negatively charged) of the same molecular size. This lack of charge selectivity suggests another difference between the intact endothelium and our in vitro system.

In summary, it appears that by physiological parameters our in vitro system is 10–100 times "leakier" than intact continuous endothelium in vivo and does not exhibit the restricted diffusion or the charge selectivity that is characteristic of such endothelium in vivo

### *Implications*

Although the currently available models of in vitro permeability (including our own) resemble intact endothelium in some ways, we found major differences in our system between the in vitro and in vivo behavior with respect to "tightness" of the barrier, size selectivity, and charge selectivity. These differences should be considered in the interpretation of any study employing a similar in vitro model of permeability. Even though large changes in permeability induced by relatively harsh injuries (such as calcium chelation) can be examined, it seems unlikely that subtle, more physiological injuries will be easily studied. The results of this study make it difficult to account for the observations that albumin can be actively and directionally transported across a cultured porcine pulmonary artery monolayer with a permeability coefficient for albumin similar to ours (24). We (unpublished observations) and others (27) have failed to duplicate these findings in cultured bovine and ovine pulmonary artery endothelial cell systems, suggesting that perhaps there may be some unique characteristics of porcine pulmonary artery endothelial cells.

The reasons for the differences between our in vitro model and native endothelium are not known for certain. One difference may be that in vivo permeability is also dependent on the characteristics of the subcellular matrix. This has been best shown in the kidney, where negatively charged molecules such as glycosaminoglycans in the glomerular capillary walls provide an electrical barrier that impedes the passage of negatively charged macromolecules (4, 30). We specifically tested the matrix produced by our endothelial cells for evidence of charge selectivity (Fig. 7) and found none, although the matrix formed in vitro may differ from that found in vivo.

Although the matrix does not seem to be the major site of restriction in our system, it is playing some role in both the electrical resistance and permeability to macromolecules. Another possible explanation may be that our estimates of in vivo permeability are incorrect. All measurements to date require certain assumptions about surface area and hydrostatic pressures. This explanation seems unlikely because of the relatively good agreement between values obtained using disparate techniques (i.e., lymph flow analysis, micropuncture, and direct measurement of tissue radioactivity). A third possibility may be that the large-vessel endothelial cells used by us and others do not closely mimic the endothelial cells of the microvascular bed. As the ability to culture capillary cells improves, this hypothesis can be tested.

On the basis of the morphological data from our system, we suggest that one additional reason for the differences between our in vitro model (and possibly between other in vitro models) and native endothelium results not from the inability of the cells to form tight junctions (as evidenced by ferritin exclusion) but from occasional gaps between adjacent cells. It is likely that this problem arises from the unnatural substrate provided by the underlying porous support. Even though cell adhesion is greatly improved by treatment of these supports with collagen and/or fibronectin, the ideal substrate remains to be developed. The use of amniotic membranes as cell supports represents one approach to this problem (9); however, the relative impermeability of this membrane and evidence that junctional anatomy remains nonphysiological suggest that another solution will be needed.

Because each investigator uses different types of endothelial cells, filter supports, and chamber configurations, no two systems are exactly alike. We would propose that some form of standardization of data reporting be adopted in future investigations. We recommend the calculation of permeability coefficients for each macromolecule tested. This mathematical term incorporates all of the relevant variables needed to describe a diffusive process (flux rates, surface area, and concentration differences) and would allow direct comparisons of in vitro and in vivo results.

Although our system was similar to others in many respects, there were also some differences. For example, our maximum resistance to dextran occurred after 14 days in culture, somewhat later than has been found by others. Our monolayer had a thicker subendothelial matrix component than has been described by some authors (10, 12). Although there may be an advantage to using collagen plus fibronectin to coat the filters, we could not find any differences. We found no evidence for asymmetric transport of albumin as has been reported by Shasby and Shasby (24). Since there may be subtle differences between systems despite similarities in morphological appearance, electrical resistance, and permeability coefficients for albumin, it would be useful for each investigator to more fully define the permeability characteristics of the particular system used. Exclusion of native ferritin could serve as a useful screening test. It may be possible that systems using other cells or substrates do have permeability characteristics more like intact endothelia.

The major finding of this study is that the current in vitro models of permeability must be viewed only as approximations of intact in vivo endothelial layers. While much useful information may be obtained from these models, their relevance to intact endothelium should be carefully weighed. Observations and information obtained from such models must be validated by other experimental techniques. As our ability to culture endothelium improves and better substrates are developed, it may be possible to more closely approximate in vivo endothelial barriers.

The authors thank Dr. James Mullin (Lankenau Hospital, Philadelphia, PA) for providing the LLC-PK$_1$ cells, Dr. Ellie Kelepouris for her assistance in measuring transendothelial resistances, Dr. John Hansen-Flaschen for his helpful criticisms, Debbie Rose and Diana Flemming for technical assistance, and Daniel Barrett for his skillful preparation of the manuscript.

This investigation was supported by National Heart, Lung, and Blood Institute Grants HL-01587 (S. M. Albelda), HL-08805 (P. M. Sampson, F. R. Haselton, J. M. McNiff, A. P. Fishman), HL-34153 (E. M. Levine, S. N. Mueller, S. K. Williams), and HL-30227 (S. K. Williams) and by National Institute on Aging Grant AG-04861 (E. M. Levine, S. N. Mueller, S. K. Williams).

Address for reprint requests: S. M. Albelda, 975 Maloney Bldg., Cardiovascular-Pulmonary Div., Hospital of the University of Pennsylvania, 3600 Spruce St., Philadelphia, PA 19104-4283.

Received 21 October 1986; accepted in final form 11 August 1987.

## REFERENCES

1. BARRY, P. H., AND J. M. DIAMOND. Effects of unstirred layers on membrane phenomenon. *Physiol. Rev.* 64: 763–872, 1984.
2. BOWMAN, P. D., S. R. ENNIS, K. E. RAREY, A. L. BETZ, AND G. W. GOLDSTEIN. Brain microvessel endothelial cells in tissue cul ture: a model for study of blood-brain barrier permeability. *Ann. Neurol.* 14: 396–402, 1983.
3. BRATZLER, R. L., G. M. CHISOLM, C. K. COLTON, K. A. SMITH, D. B. ZILVERSMIT, AND R. S. LEES. The distribution of labeled albumin across the rabbit thoracic aorta in vivo. *Circ. Res.* 40: 182–190, 1977.
4. BRENNER, B. M., T. H. HOSTETTER, AND H. D. HUMES. Glomerular permselectivity: barrier function based on discrimination of molecular size and charge. *Am. J. Physiol.* 234 (*Renal Fluid Electrolyte Physiol.* 3): F455–F460, 1978.
5. BRUNS, R. R., AND G. E. PALADE. Studies on blood capillaries. II. Transport of ferritin molecules across the wall of muscle capillaries. *J. Cell Biol.* 37: 277–299, 1968.
6. CEREIJIDO, M., J. J. BOLIVAR, L. GONZALEZ MARISCAL, AND G. AVILA. Cultured monolayers as model systems for ion transport across epithelial and endothelial membranes. State of the art lecture. *Hypertension Dallas* 8, *Suppl.* I: I-22–I-29, 1986.
7. CRONE, C., AND O. CHRISTENSEN. Electrical resistance of a capillary endothelium. *J. Gen. Physiol.* 77: 349–371, 1981.
8. CRONE, C., AND S. P. OLESEN. The electrical resistance of brain capillary endothelium. *J. Physiol. Lond.* 316: 53P–54P, 1981.
9. FURIE, M. B., E. B. CRAMER, B. L. NAPRSTEK, AND S. C. SILVERSTEIN. Cultured endothelial cell monolayers that restrict the transendothelial passage of macromolecules and electrical current. *J. Cell Biol.* 98: 1033–1041, 1984.
10. GARCIA, J. G. N., A. SIFLINGER-BIRNBOIM, R. BIZIOS, P. J. DEL VECCHIO, J. W. FENTON II, AND A. R. MALIK. Thrombin-induced increase in albumin permeability across the endothelium. *J. Cell. Physiol.* 128: 96–104, 1986.
11. GOSPODAROWICZ, D., AND C. ILL. Extracellular matrix and control of proliferation of vascular endothelial cells. *J. Clin. Invest.* 65: 1351–1364, 1980.
12. HARLAN, J. M., B. R. SCHWARTZ, M. A. REIDY, S. M. SCHWARTZ,

H. D. OCHS, AND L. A. HARKER. Activated neutrophils disrupt endothelial monolayer integrity by an oxygen radical-independent mechanism. *Lab. Invest.* 52: 141–150, 1985.

13. HÜTTNER, I., M. BOUTET, AND R. H. MORE. Studies on protein passage through arterial endothelium. I. Structural correlates of permeability in rat arterial endothelium. *Lab. Invest.* 28: 672–677, 1973.
14. HÜTTNER, I., M. BOUTET, AND R. H. MORE. Studies on protein passage through arterial endothelium. II. Regional differences in permeability to fine structural protein tracers in arterial endothelium of normotensive rat. *Lab. Invest.* 28: 678–685, 1973.
15. JOYNER, W. L., AND F. E. CURRY. Measurement of albumin permeability coefficients in single capillaries of the hamster mesentery (Abstract). *Federation Proc.* 45: 583, 1986.
16. LANKEN, P. N., J. H. HANSEN-FLASCHEN, P. M. SAMPSON, G. G. PIETRA, F. R. HASELTON, AND A. P. FISHMAN. Passage of uncharged dextrans from blood to lung lymph in awake sheep. *J. Appl. Physiol.* 59: 580–591, 1985.
17. MULLIN, J. M., L. FLUK, AND A. KLEINZELLER. Basal-lateral transport and transcellular flux of methyl α-D-glucoside across LLC-PK1 renal epithelial cells. *Biochim. Biophys. Acta* 885: 233–239, 1986.
18. NAVAB, M., G. P. HOUGH, J. A. BERLINER, J. A. FRANK, A. M. FOGELMAN, M. E. HABERLAND, AND P. A. EDWARDS. Rabbit beta-migrating very low density lipoprotein increases endothelial macromolecular transport without altering electrical resistance. *J. Clin. Invest.* 78: 389–397, 1986.
19. O'DONNELL, M. P., AND F. F. VARGAS. Electrical conductivity and its use in estimating an equivalent pore size for arterial endothelium. *Am. J. Physiol.* 250 (*Heart Circ. Physiol.* 19): H16–H21, 1986.
20. RENKIN, E. M. Multiple pathways of capillary permeability. *Circ. Res.* 41: 735–743, 1977.
21. ROSEN, E. M., S. N. MUELLER, J. P. NOVERAL, AND E. M. LEVINE. Proliferative characteristics of clonal endothelial cell strains. *J. Cell. Physiol.* 107: 123–137, 1981.
22. ROSEN, E. M., J. P. NOVERAL, S. N. MUELLER, AND E. M. LEVINE. Regulation of angiotensin I-converting enzyme activity in serially cultivated bovine endothelial cells. *J. Cell. Physiol.* 122: 30–38, 1985.
23. SCHWARTZ, S. M., AND E. P. BENDITT. Studies on aortic intima. I. Structure and permeability of rat thoracic aortic intima. *Am. J. Pathol.* 66: 241–264, 1972.
24. SHASBY, D. M., AND S. S. SHASBY. Active transendothelial transport of albumin. *Circ. Res.* 57: 903–908, 1985.
25. SHASBY, D. M., AND S. S. SHASBY. Effects of calcium on transendothelial albumin transfer and electrical resistance. *J. Appl. Physiol.* 60: 71–79, 1986.
26. SIFLINGER-BIRNBOIM, A., P. J. DEL VECCHIO, J. A. COOPER, F. A. BLUMENSTOCK, J. M. SHEPARD, AND A. B. MALIK. Molecular sieving characteristics of the cultured endothelial monolayers. *J. Cell. Physiol.* 132: 111–117, 1987.
27. SIFLINGER-BIRNBOIM, A., P. J. DEL VECCHIO, J. A. COOPER, AND A. B. MALIK. Transendothelial albumin flux: evidence against active transport of albumin. *J. Appl. Physiol.* 61: 2035–2039, 1986.
28. TAYLOR, A. E., AND D. N. GRANGER. Equivalent pore modeling: vesicles and channels. *Federation Proc.* 42: 2440–2445, 1983.
29. TERRITO, M., J. A. BERLINER, AND A. M. FOGELMAN. Effect of monocyte migration on low density lipoprotein transport across aortic endothelial cell monolayers. *J. Clin. Invest.* 74: 2279–2284, 1984.
30. VEHASKARI, V. M., C.T-C. CHANG, J. K. STEVENS, AND A. M. ROBSON. The effects of polycations on vascular permeability in the rat. A proposed role for charge sites. *J. Clin. Invest.* 73: 1053–1061, 1984.